Atmos. Chem. Phys., 23, 9585–9595, 2023
https://doi.org/10.5194/acp-23-9585-2023

Atmospheric Chemistry and Physics
Open Access
EGU

Distinct photochemistry in glycine particles mixed with different atmospheric nitrate salts

Zhancong Liang[1,2], Zhihao Cheng[1], Ruifeng Zhang[1,2], Yiming Qin[1], and Chak K. Chan[1,3]

[1]School of Energy and Environment, City University of Hong Kong, Hong Kong SAR, China
[2]Shenzhen Research Institute, City University of Hong Kong, Shenzhen, China
[3]Division of Physical Science and Engineering, King Abdullah University of Science and Technology, 23955-6900 Thuwal, Saudi Arabia

Correspondence: Chak K. Chan (chak.k.chan@cityu.edu.hk, chak.chan@kaust.edu.sa)

Received: 21 May 2023 – Discussion started: 1 June 2023
Revised: 14 July 2023 – Accepted: 16 July 2023 – Published: 29 August 2023

Abstract. Particulate free amino acids (FAAs) are essential components of organonitrogen that have critical climate impacts, and they are usually considered stable end-products from protein degradation. In this work, we investigated the decay of glycine (GC) as a model FAA under the photolysis of different particulate nitrate salts using an in situ Micro-Raman system. Upon cycling the relative humidity (RH) between 3 % and 80 % RH, ammonium nitrate (AN) and GC mixed particles did not exhibit any phase change, whereas sodium nitrate (SN) and GC mixed particles crystallized at 60 % and deliquesced at 82 % RH. Under light illumination at 80 % RH, AN + GC particles showed almost no spectral changes, while rapid decays of glycine and nitrate were observed in SN + GC particles. The interactions between nitrate and glycine in AN + GC particles suppressed crystallization but also hindered nitrate photolysis and glycine decay. On the other hand, glycine may form a complex with Na^+ in deliquescent SN + GC particles and allow unbonded nitrate to undergo photolysis and trigger glycine decay, though nitrate photolysis was greatly hindered upon particle crystallization. Our work provides insights into how FAAs may interact with different nitrate salts under irradiation and lead to distinct decay rates, which facilitates their atmospheric lifetime estimation.

1 Introduction

Free amino acids (FAAs) are essential components of atmospheric particles with wide sources, including direct bio-emissions, degradation of proteinaceous materials, and biomass burning (Ren et al., 2018; Matos et al., 2016; Zhu et al., 2021; X. Li et al., 2022; F. Liu et al., 2017). The concentrations of FAAs in terrestrial and marine near-surface atmospheres generally range from a few to several hundred nanograms per cubic meter (Helin et al., 2017; Matos et al., 2016). FAAs play important roles in the climate-related properties of atmospheric particles, such as hygroscopicity and cloud condensation nuclei (CCN) activity (Chan et al., 2005; Kristensson et al., 2010; Marsh et al., 2017) and atmospheric nitrogen cycling (Mopper and Zika, 1987). Besides, FAAs support biological activity in the aerosol particles (Helin et al., 2017) and impact human health after inhalation (Hu et al., 2020). While the importance of atmospheric FAAs was well recognized, previous atmospheric studies mainly focused on the regional and seasonal variations in the abundance of particulate FAAs (Ren et al., 2018; Helin et al., 2017; Song et al., 2017). FAAs were suggested as the stable end-products of the degradation of protein (X. Li et al., 2022). However, a few studies have reported the reactions of atmospheric FAAs and carbonyl compounds to form light-absorbing compounds via oligomerization under dark conditions (De Haan et al., 2011; Haan et al., 2009). The photochemical evolution of FAAs remains less explored.

Nitrate is ubiquitous in atmospheric particles (Chan and Yao, 2008), and it can generate various oxidants, including OH radicals, via photolysis (Gen et al., 2022; Scharko et al., 2014; Benedict et al., 2017). Oxidants

from particulate nitrate photolysis could oxidize gaseous precursors to secondary inorganic and organic aerosols (Gen et al., 2022; Gen et al., 2019; Zhang et al., 2021, 2022) and change the morphology of the particles (Liang et al., 2021). Correlation analysis of field measurements suggests that particulate FAAs and nitrate could be from the same sources (Xu et al., 2019; Gao et al., 2021), and there were also laboratory studies on the hygroscopicity of FAA–nitrate mixed particles (Ashraf et al., 2021; Wang et al., 2018). While external oxidants such as gaseous ozone and OH radicals need to diffuse across the interfacial layers, nitrate photolysis generates oxidants inside the particles (Liang et al., 2021). Particulate nitrate photolysis may afford effective FAA oxidation. However, it is unclear how FAAs would chemically evolve under nitrate photolysis, though it is well known that OH radicals can react with FAAs in water treatment research (Berger et al., 1999; Acero et al., 2000). Recently, Wen et al. (2022) demonstrated that aqueous OH oxidation could be a significant sink of atmospheric FAAs. Nevertheless, while these results were helpful for diluted aqueous systems, the reactions in the particle phase could be different due to the elevated concentrations that facilitate molecular interactions. Specifically, glycine (GC), which is the most abundant FAA in atmospheric particles with a mole ratio of GC to total FAAs = 0.17–0.49 (X. Li et al., 2022; Ren et al., 2018; Song et al., 2017; Zhang and Anastasio, 2003; Zhu et al., 2020), could bind with atmospheric-relevant inorganics such as sulfate and nitrate (Ashraf et al., 2021). The phase state of the particles can also play an essential role in nitrate photolysis (Liang et al., 2021; Gen et al., 2022).

In this paper, we first performed relative humidity (RH) cycling to characterize the phase transition behavior of mixed particles of ammonium nitrate (AN) and glycine, as well as sodium nitrate (SN) and glycine. Then, we examined the photochemistry of glycine triggered by the photolysis of AN and SN at different RH levels. The phase transition behaviors of AN + GC and SN + GC mixed particles and the kinetics of glycine decay under ultraviolet (UV) illumination are significantly different.

2 Experiment

2.1 Photochemical aging of droplets

Mixed solutions (1 wt %) of AN (> 99 %; Sigma-Aldrich) or SN (> 99 %; Acros Organics) and glycine (biological analysis level; ChemCruz™) were prepared in deionized water (Milli-Q). We used a mole ratio of 1 : 1 for glycine and nitrate in all our experiments. Mixed solutions were atomized using a piezoelectric particle generator (model 201; Uni-Photon Systems, Inc.) coupled with a quartz tip (MicroFab Technologies Inc.; orifice diameter of 80 µm). Droplets were deposited on a hydrophobic fluorocarbon substrate (model 5793; YSI Incorporated) and placed in an aerosol flow cell (Liang et al., 2021, 2022b). The flow cell has two windows for in situ Raman analysis (top) and UV illumination (bottom). The schematic of the experimental setup is shown in Fig. S1 in the Supplement. The RH inside the flow cell was controlled by mixed dry and wet synthetic air (Linde plc) and monitored by a digital RH sensor (HC2-C05; ROTRONIC AG, Switzerland). The deposited droplets were photolyzed for 8 h, using a 300 nm light-emitting diode (LED) lamp (M300L4; Thorlabs, Inc.). The photon flux received by deposited particles in the flow cell was determined to be 1.2×10^{15} photons per centimeter squared per second by 2-nitrobenzaldehyde (2NB; > 99.0 %; Acros Organics). A detailed description can be found in our previous work (Liang et al., 2021). The effective incident light flux used in our study was comparable to that received by nitrate in the atmosphere on a typical clean day.

2.2 In situ Raman and microscopic characterization

A Raman spectrometer (EnSpectr R532; Enhanced Spectrometry, Inc.) with a 20–30 mW 532 nm laser and holographic diffraction grating with 1800 grooves per millimeter was used to characterize the particle in situ during the phase transition behavior measurement and photoreactions of the particles. The Raman spectrometer was coupled with an optical microscope (CX41; Olympus LS) to acquire Raman spectra at 100–4000 cm^{-1} at a resolution of 4 cm^{-1}. A 50× objective lens with a numerical aperture of 0.35 (SLMPLN 50X; Olympus LS) was used to guide the laser onto the particles. For the phase transition measurements, we evaporated and then humidified the particles by decreasing and increasing the RH gradually. Images of the particles were captured, and the Raman spectra were recorded after equilibrium was reached. The size of the equilibrated droplets at 80 % RH was 41 ± 15 µm. The in situ Raman analysis focused on single particles of ∼ 40 µm, while approximately 1300 particles were used for offline analysis (will be discussed later). Particle composition during photoreactions was monitored using Raman measurement every hour for 8 h. The integration time for each spectrum was 5 s. Glycine absorbs light at below 260 nm, but it can form light-absorbing mesoclusters in droplets and trigger photosensitization to degrade itself at 532 nm, which is our Raman excitation wavelength (Ishizuka et al., 2023). However, this mechanism played a minor role in our system, as no glycine decay in GC droplets without nitrate at 80 % RH was found.

2.3 Offline chemical analysis of particle extracts

Particle-loaded substrates were extracted using 1 mL Milli-Q water after photoreactions. The water extract was analyzed by ion chromatography (IC). The IC protocol was the same as in our previous work (Liang et al., 2022c). After equilibrating at 80 % RH, the initial particle pH was measured by pH indicator paper combined with RGB-based

colorimetric analyses using a model of $G - B$ (G minus B) vs. pH^2, according to Craig et al. (2018). The particles were considered to be at equilibrium when the size became unchanged ($\pm 2\,\%$) for 30 min. The nitrate and glycine concentrations were obtained according to Eq. (1), where a is the scaling factor determined by calibration, and A refers to the integrated area of the corresponding peak using Gaussian fitting (Igor Pro 8). The wavenumber ranges used for integration were 850–950 cm^{-1} for glycine and 980–1100 cm^{-1} for nitrate, respectively.

$$[X]_{\text{particle}} = a \times (A(X)/A(\text{OH})_{3400\,\text{cm}^{-1}}), \quad (1)$$

where X is nitrate or glycine, and $A(\text{OH})_{3400\,\text{cm}^{-1}}$ refers to the main peak of water.

2.4 Estimation of nitrate photolysis rate constant and percentage glycine decay

The maximum RH reached in the flow cell was 96 %, which yields a solute concentration in particles higher than 1 M. Thus, kinetic data of diluted systems (0.01, 0.1, and 0.5 M) were obtained from aqueous solutions. The schematic of the custom-made aqueous reactor is shown in Fig. S2. Synthetic air was introduced to the aqueous reactor at 0.1 L min^{-1}. The AN + GC and SN + GC solutions (0.01, 0.1, or 0.5 M) were added to the aqueous reactor and illuminated by 300 nm LED through a quartz window at the top of the reactor. The photon flux received by the solution was 0.7×10^{15} photons per centimeter squared per second by 2NB, which is $\sim 60\,\%$ of the flux found for deposited particles in the flow cell. We sampled the aliquots from the aqueous solution after 13.3 h of irradiation. After sampling, the glycine concentration was immediately determined using the precolumn derivatization high-performance liquid chromatography (HPLC) method described by Matsumoto et al. (2021). The nitrate concentration was determined by IC.

The apparent nitrate photolysis rate constant J (s^{-1}) was estimated as Eq. (2). J depends on the light intensity, quantum yield, and absorption cross section of nitrate (George et al., 2015).

$$\frac{\mathrm{d}[NO_3^-]}{\mathrm{d}t} = -J \times [NO_3^-] \quad (2)$$

This is a low estimate of J, since glycine oxidation likely generates secondary nitrate (Berger et al., 1999). We estimated the percentage of GC decay to indicate the effectiveness of the decay under different conditions, based on [GC] measured before and after irradiation (after 8 h for deposited particles and 13.3 h for solutions). The percentage of GC decay in crystalline SN + GC particles was estimated directly by the GC peak area as the water peak was not available.

2.5 Estimation of water-to-glycine mole ratio

Though still under debate, the water-to-glycine mole ratio was reported to play a crucial role in affecting the configuration of glycine (Aikens and Gordon, 2006; Tortonda et al., 1996). Here, we estimate the water-to-glycine mole ratio in AN + GC and SN + GC particles and discuss the potential form of glycine, which may play a role in photochemistry.

$$\begin{aligned} \text{GF} = \frac{V_{\text{wet}}}{V_{\text{dry}}} &= \frac{(m_{\text{w}} + m_{\text{dry}})/\rho_{\text{wet}}}{m_{\text{dry}}/\rho_{\text{dry}}} \\ &= \left(1 + \frac{m_{\text{w}}}{m_{\text{dry}}}\right) \times \frac{\rho_{\text{dry}}}{\rho_{\text{wet}}} \\ &= \left(1 + \frac{M_{\text{w}}}{M_{\text{dry}}} \times \frac{n_{\text{w}}}{n_{\text{dry}}}\right) \times \frac{\rho_{\text{dry}}}{\rho_{\text{wet}}} \end{aligned} \quad (3)$$

$$\text{GF} = \frac{V_{\text{wet}}}{V_{\text{dry}}} = \frac{(d_{\text{wet}})^3}{(d_{\text{dry}})^3} \quad (4)$$

GF is the volumetric growth factor (i.e., the volume ratio of a wet droplet to dry particles at a specific RH), and V, m, ρ, n, M, and d represent the volume, mass, density, mole number, molar mass, and diameter of the particles, respectively. The subscripts dry, wet, and w denote dry particles (i.e., solutes), wet particles, and water, respectively. Note that the estimation of GF using Eq. (4) assumes spherical particles on the hydrophobic substrate, and d_{dry} was estimated by averaging two measured diameters from orthogonal directions. For an initially non-spherical particle to form a droplet upon RH increase, the estimation of GF by Eq. (4) would be a slight overestimation (Matsumura and Hayashi, 2007). Then, the water-to-glycine mole ratio (WGR) can be obtained by the following:

$$\text{WGR} = 2 \times \frac{n_{\text{w}}}{n_{\text{dry}}} = 2 \times \left[\frac{(d_{\text{wet}})^3}{(d_{\text{dry}})^3} \times \frac{\rho_{\text{wet}}}{\rho_{\text{dry}}} - 1\right] \times \frac{M_{\text{dry}}}{M_{\text{w}}}. \quad (5)$$

The mean molar mass of glycine and the nitrate salts was used as M_{dry}. ρ_{dry} of SN + GC particles was available in the literature (Suresh et al., 2010), while ρ_{dry} of AN + GC particles and ρ_{wet} of both particles were estimated based on the simple volume additivity rule (Eq. 6) (Ha and Chan, 1999; Tang, 1997). ρ_{GC}, ρ_{AN}, and ρ_{SN} were the densities of pure aqueous solutions at the total solute mass fraction X of the mixed solution obtained from the literature (Venkatesu et al., 2007) and the Extended Aerosol Inorganics Model (E-AIM) prediction (Clegg et al., 1998).

$$\frac{1}{\rho_{\text{wet}}} = \frac{X_{\text{GC}}}{\rho_{\text{GC}}} + \left(\frac{X_{\text{AN}}}{\rho_{\text{AN}}} \text{ or } \frac{X_{\text{SN}}}{\rho_{\text{SN}}}\right) \quad (6)$$

3 Results and discussion

3.1 Phase transition behavior of nitrate–glycine mixed particles

We first examined the phase transition behavior of the nitrate–glycine mixed particles without UV illumination. Figure 1 shows the images and Raman spectra of AN + GC and SN + GC particles undergoing an evaporation–humidification cycle. The black line in Fig. 1b shows the Raman spectra of an AN + GC mixed droplet at 85 % RH. The $\upsilon(NO_3^-)$ peaks are at ∼ 730 and ∼ 1040 cm^{-1} (Ling and Chan, 2007). The C–C stretching and C–N stretching peaks are located at ∼ 890 cm^{-1} (Socrates, 2004). In 1300–1450 cm^{-1}, there are overlapping peaks from C–H vibration in different chemical environments. Peaks at 2970 and 3020 cm^{-1} show the antisymmetric and symmetric stretching of CH_2, respectively. The two broad peaks at 3250 and 3450 cm^{-1} are from the stretching of OH, indicating the presence of liquid water (Furić et al., 1992). The $\upsilon(NH_4^+)$ also contributed to the peak at 3250 cm^{-1}.

Upon RH decrease from 85 % to 3 %, the AN + GC particle shrank, but remained spherical, suggesting that the particle gradually lost water and became a dry amorphous solid (Fig. 1a). Crystallization did not occur, since there was no sudden decrease in the full width at half maximum (FWHM) of the nitrate and glycine peaks (Liang et al., 2021; Surovtsev et al., 2012; Liang et al., 2022a). Besides, the 3450 cm^{-1} peak diminished, suggesting that the particle lost water without phase transition, which is consistent with the literature (Wang et al., 2022). Although some studies reported an absence of efflorescence RH (ERH) in pure AN (Zuend et al., 2011; Lightstone et al., 2000), the ERH of pure GC was 61.7 % (Wang et al., 2022). Adding crystallizable organics such as succinic acid to AN would also promote its crystallization (Lightstone et al., 2000). The absence of a phase transition in the AN + GC particles can be attributed to the chaotropic nature of AN, which results in the "salting-in" effect of glycine and the gradual evaporation of water (Ashraf et al., 2021) without crystallization. As an amino acid, GC has a proton-donating carboxyl (COOH) group and a proton-accepting amino (NH_2) group. The latter can form hydrogen bonding with nitrate to suppress crystallization (Wang et al., 2022). This was supported by the FWHM increases in the GC and nitrate peaks as RH decreased (Fig. S3), due to intensified molecular interaction. The particles are likely dehydrated at 3 % RH due to the absence of OH peaks from 3200 to 3500 cm^{-1}. As RH increased, the particle took up water again and grew. There was no spectral change, other than the increase in the O–H peak at 3450 cm^{-1} (Guo et al., 2010).

For the SN + GC particle, the particle size decreased as RH decreased from 84 % to 60 % (Fig. 1c). The black line in Fig. 1d shows the Raman spectrum of an SN + GC mixed droplet at 84 % RH, which is almost identical to that

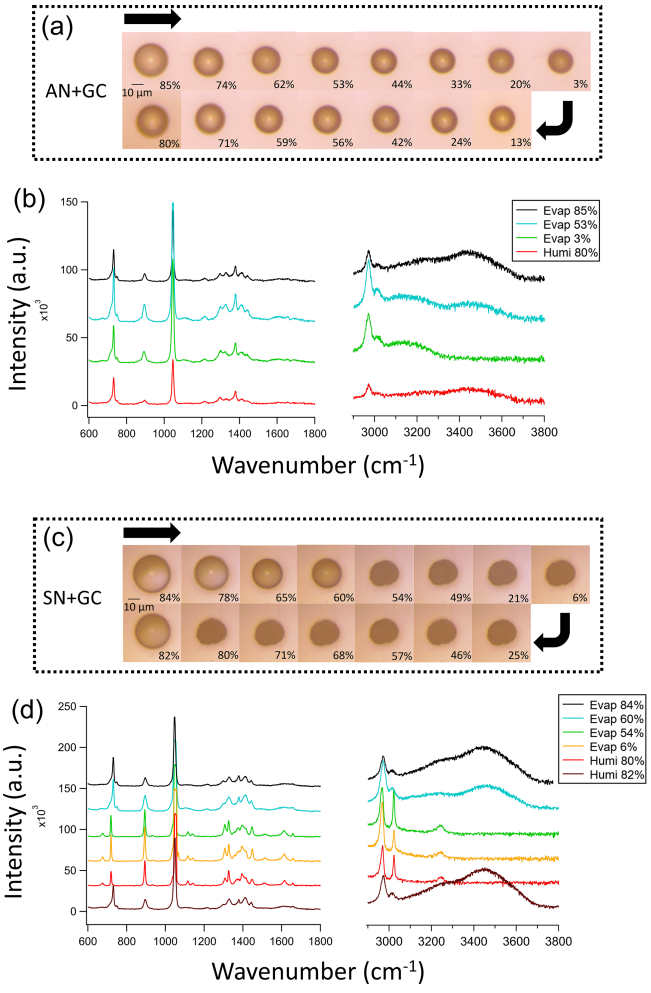

Figure 1. Images and Raman spectra of the mixed **(a, b)** AN + GC particles and **(c, d)** SN + GC particles during an evaporation–humidification cycle. The arrows in panels **(a)** and **(c)** show the changes in the relative humidity.

of an AN + GC mixed droplet at 85 % RH. Interestingly, different from AN + GC particles, a phase transition from a droplet to a crystalline solid was observed at 54 % RH. The Raman spectra show a redshift of the nitrate peak from 730 to 710 cm^{-1} and a blueshift in the 1046 cm^{-1} peak to 1051 cm^{-1}, which is attributable to the formation of glycine–sodium nitrate crystal (GSN; Fig. S4; Gujarati et al., 2015). Two new peaks are attributed to the $-NH_3^+$ rocking mode at 1100 cm^{-1} after crystallization, which is likely due to the more restricted vibration in the crystalline lattice than in the aqueous droplet (Jentzsch et al., 2013). The FWHM of the CH_2 peaks at 1300 and 3020 cm^{-1} also decreased after crystallization. As RH further decreased to 3 %, no noticeable change in appearance was observed. The SN + GC crystal returned to a droplet at 82 % RH after humidification.

3.2 Photochemistry of glycine with different nitrate salts

The different phase transition behaviors observed in AN + GC and SN + GC particles reflect the role of molecular interaction in determining the physicochemical properties of the particles. To examine if such interactions could play a role in the chemical reactivity of the particles, we exposed the AN + GC and SN + GC particles to UV irradiation at 80 % RH.

The Raman spectral characteristics of AN + GC particles only show slight changes from 0 to 8 h of irradiation (Fig. 2a). Offline IC analysis also shows that no new product formed (Fig. S5). However, the spectra of SN + GC particles show apparent changes upon light irradiation. Overall, glycine peaks, including C–N/C–C (890 cm^{-1}) and CH_2 (1325, 1425, 2970, and 3020 cm^{-1}; Kumar et al., 2005), decreased, but peaks at 920 (C–C) and 1350 cm^{-1} (C–O) attributable to acetate and formate, respectively, emerged (Figs. S5 and S6; Zhang et al., 2021). The rising peaks at 1350 and 2925 cm^{-1} correspond to amide and ammonia and/or amine (Philipsen et al., 2013; Socrates, 2004). Besides, nitrite was also found in the particle extracts using IC. Nitrate photolysis directly generates HNO_2/NO_2^- (Gen et al., 2022), and the reaction between the two other nitrate photolysis products, NO_2 and OH^-, would also form nitrite (Pei et al., 2023).

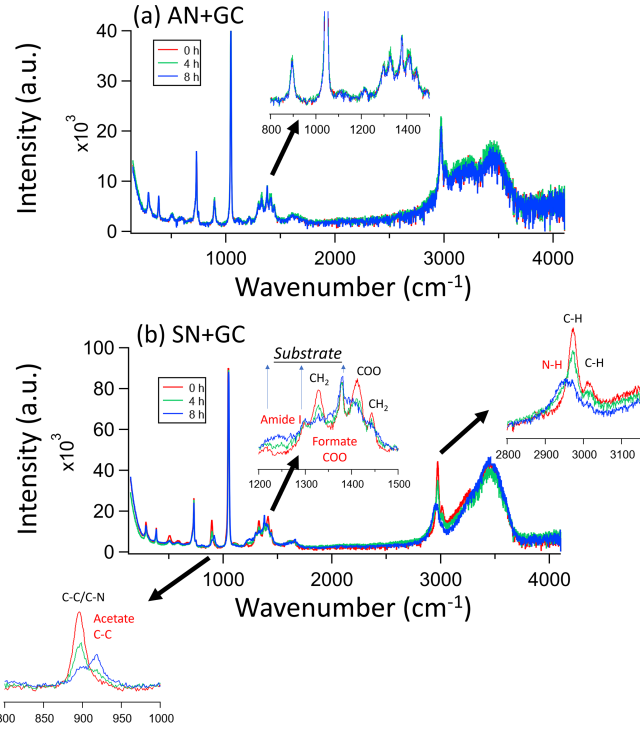

Figure 2. Raman spectral evolution of **(a)** AN + GC and **(b)** SN + GC particles after 0, 4, and 8 h irradiation. The insets are expanded regions of the SN + GC particle spectra in the ranges of [800,1000], [1200,1500], and [2800, 3150] (units in cm^{-1}). The red annotations denote the peaks from products. The spectra were normalized by the substrate peak at around 1400 cm^{-1}.

3.3 Nitrate photochemistry of AN + GC and SN + GC particles

The efficiencies of nitrate photolysis in the two mixed systems were different. The fitted apparent nitrate photolysis rate constant of SN + GC particles at 80 % RH was $9 \times 10^{-6}\ s^{-1}$ ($R^2 = 0.95$), which is 4.5-fold higher than that of AN + GC particles (Fig. S7). The nitrate photolysis rate constant in SN + GC particles was comparable to SN particles without glycine ($1.2 \times 10^{-5}\ s^{-1}$), which indicates that glycine has a minor suppression effect on SN photolysis. The faster nitrate photolysis in SN + GC particles likely contributed to the faster glycine decay, and the different molecular interactions may explain the discrepancy in nitrate photolysis rate constant between SN + GC and AN + GC particles.

For instance, amino acid nitrate can form through (water-mediated) hydrogen bonding between nitrate from AN and the protonated amino group of glycine (Fig. 3a; Wang et al., 2022; Ashraf et al., 2021). As a result, the amino acids and nitrate ions in the droplet are bounded in an extensive three-dimensional, hydrogen-bonded matrix (Wang et al., 2022) in which nitrate photolysis could be hindered (Vimalan et al., 2010). We envision that such interactions exist in our AN + GC system. On the other hand, the COO^- of glycine can bind with SN via Na^+ directly to form a bidentate complex (Fig. 3a; Moision and Armentrout, 2002; Aziz et al., 2008; Selvarani et al., 2022), thus leaving nitrate unbonded. The nitrate peak in SN + GC particles split into two (Fig. 3b). One has the same Raman shift as nitrate in AN + GC, which is likely bonded nitrate, while the other peak at 1046 cm^{-1} was attributable to unbonded aqueous nitrate (Liang et al., 2022a), which can undergo photolysis to form a wealth of oxidants that lead to glycine decay (Fig. 3a). The single symmetric nitrate peak, small J, and minor glycine decay of AN + GC particles suggested a negligible fraction of unbonded nitrate. However, we also note that the exact molecular configuration in concentrated particles can be much more complicated than the illustrative example shown in Fig. 3a. Detailed investigations of quantum chemistry and molecular dynamic simulation with appropriate parameterization for non-ideal solutions are required.

One would expect that these effects are more evident at lower RH (but before crystallization), with higher solute concentrations and fewer water molecules. Figure 4a shows the percentage of GC decay after irradiation as a function of the initial solute concentrations. At 0.01 M, the percentage of GC decay is approximately 5 % in both AN + GC and SN + GC solutions (Fig. 4a). However, as the initial solute concentration increased from 0.01 M to ∼ 7.6 M, the percentage of GC decay in SN + GC particles increased

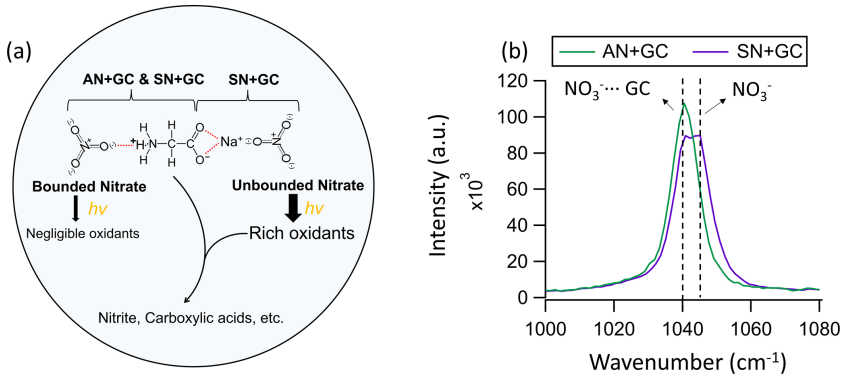

Figure 3. **(a)** A plausible schematic of the photochemical processes and molecular interactions in AN + GC and SN + GC particles. Dashed red lines indicate the binding. The binding between AN + GC may be mediated by water (Ashraf et al., 2021). **(b)** The Raman peak of the nitrate of AN + GC and SN + GC particles at 80 % RH before illumination. The spectra were normalized by the substrate peaks.

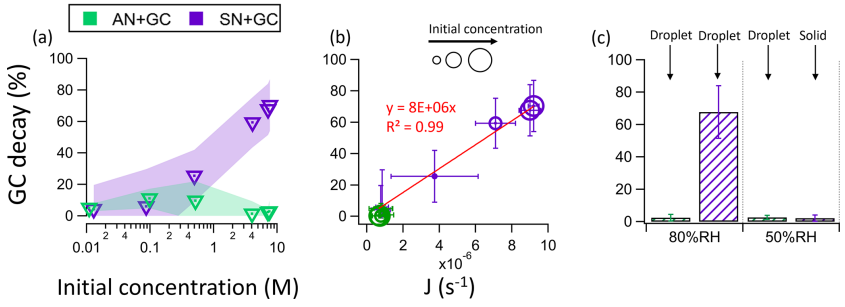

Figure 4. **(a)** The percentage decay of GC as a function of the initial concentration of GC in AN + GC and SN + GC equimolar mixtures. The shaded regions represent the standard deviations. **(b)** The correlation between the nitrate photolysis rate constant (J) and the percentage of GC decay. **(c)** The percentage of GC decay in AN + GC and SN + GC particles at 80 % and 50 % RH.

by more than 1 order of magnitude to 70 %, while that of the AN + GC particles remained small. The apparent nitrate photolysis rate constant J shows a good correlation with the percentage of GC decay ($R^2 = 0.99$; Fig. 4b), which suggests that nitrate photolysis is the key driver for the glycine decay.

The different reactivity of glycine between SN + GC and AN + GC particles may also contribute to the distinct photochemistry. For instance, glycine can be ionized into different forms according to the local conditions, including cationic, zwitterionic, and anionic polymers of different reactivities (Aikens and Gordon, 2006). The term zwitterionic denotes the charge-separated form of amino acids in aqueous solutions and in crystalline states (e.g., NH_3^+–CH_2–COO^-). Several possible zwitterionic conformers of glycine have been proposed with the addition of one to three water molecules (Krauklis et al., 2020). The rate of anionic glycine reacting with OH radicals is 2 orders of magnitude higher than that of zwitterionic glycine (Berger et al., 1999; Buxton et al., 1988), while that of zwitterionic glycine is several times higher than cationic glycine. These differences were due to the increased energy barriers for oxidation upon protonation (Wen et al., 2022). However, the protonation constants of glycine in concentrated solution were difficult to define. Qualitatively, a possibly lower degree of glycine protonation in SN + GC particles than AN + GC particles might enhance the reactivity of glycine.

We also note that the initial water-to-glycine mole ratios were higher for AN + GC particles (6) than SN + GC particles (2), and sodium has a higher hydration number (6; Medoš et al., 2019) than ammonium (4; Guo et al., 2020). Therefore, the availability of free water in AN + GC particles is likely higher than in SN + GC particles. This could affect the configuration of glycine dimers or trimers, such as the possible complexation of charge interactions between the anionic carboxylate and the cationic$-NH_3^+$ groups. These factors could also modulate the photoreactivity of glycine.

Though no phase transition occurred at RH below 60 %, the percentage of GC decay in AN + GC particles was very small (Fig. 4c). On the other hand, SN + GC particles crystallized at 50 %, and the percentage of GC decay after 8 h irradiation became < 5 %, which is much smaller than that at 80 % RH (Fig. 4c). Such a reduction in glycine decay was likely due to the ineffective photolysis of nitrate in the crystalline lattices (Asher et al., 2011). The crystalline lattices greatly constrain the diffusion of nitrate photolysis

products and facilitate their recombination to form nitrate, resulting in a very low photolysis quantum yield.

4 Atmospheric implications

This work showed the distinct decay characteristics of glycine as a model FAA in AN and SN particles under the light. AN + GC particles did not crystalize at RH as low as 3 %, while SN + GC did at 50 %–60 % RH. On the other hand, glycine in AN + GC particles exhibited a much slower decay than in SN + GC particles under UV irradiation. A plausible explanation was the water-mediated bonding between nitrate and GC in AN + GC particles that suppressed crystallization but also hindered nitrate photolysis from generating oxidants and reduced the reactivity of glycine. In contrast, some unbonded nitrate existed in deliquescent SN + GC particles to undergo photolysis and triggered glycine decay effectively, though it was significantly hindered once the particle crystallized. Besides glycine, alanine (Ala) was another major FAA in atmospheric particles (mole ratio of Ala to total FAAs is 0.07–0.17; Matos et al., 2016; Zhu et al., 2020; Zhang and Anastasio, 2003). After 8 h irradiation, we also found evident Ala decay in deliquescent SN + Ala particles but not in AN + Ala ones (Fig. S8).

It is widely reported that nitrate dominantly exists as SN in the coarse-mode aged sea salt particles and AN in the fine-mode particles (Zhuang et al., 1999a, b). Concentrations of FAAs in the coarse mode were ∼ 10 times higher than that in the fine mode (Helin et al., 2017), which implies that the FAAs plausibly co-existed with SN in atmospheric particles and were subjected to oxidation triggered by effective SN photolysis.

Similar to what we found in SN + GC particles, it has been reported that particulate nitrate photolysis rate constants (i.e., $10^{-5}\,s^{-1}$) can be 2 orders of magnitude higher than nitrate photolysis in cloud and fog water (i.e., $10^{-7}\,s^{-1}$), which is likely due to the reduced surface cage (Gen et al., 2022). H_2O_2 photolysis ($J = \sim 2 \times 10^{-6}\,s^{-1}$) was considered to be the primary OH source in aqueous cloud water (Bianco et al., 2015), and the aqueous-phase reactions with OH were reported as an important sink of the cloud FAAs (Wen et al., 2022). However, the small liquid water content in aerosol particles limits the partitioning of H_2O_2 into the particle phase. Taking particulate $[H_2O_2]$ and $[NO_3^-]$ as $0.1\,ng\,\mu g^{-1}$ and $0.2\,\mu g\,\mu g^{-1}$ (per $PM_{2.5}$ mass; Xuan et al., 2020; Cheng et al., 2016; Y. Li et al., 2022), respectively, the OH generation from particulate nitrate photolysis could be 4 orders of magnitude higher than from H_2O_2 photolysis. Other oxidants from nitrate photolysis, such as nitrite and HONO, can also react with FAAs to promote their decay via N nitration (Kitada et al., 2020). As shown in Fig. 3a, the complexation of glycine with the cation could be crucial for allowing free nitrate for photolysis. Other atmospheric cations, such as potassium, magnesium and calcium, can also form complexes with the carboxylic group of amino acids (Case et al., 2020; Lester et al., 2010; Tang and Skibsted, 2016). The pH of global ambient aerosol can span from 0–6 (Weber et al., 2016; M. Liu et al., 2017), which means that amino acids can exist in both cationic ($0 < pH < 2$) and zwitterionic ($2 < pH < 10$) forms (Locke and McIver, 1983; Stroud et al., 1983). Previous studies have reported that complexation is enhanced for cationic amino acids due to the protonation (Moision and Armentrout, 2002).

Overall, this paper sheds light on the potential role of particulate nitrate photolysis in the sink of the atmospheric FAAs, which impacts the cycling of atmospheric organic nitrogen. The reaction rate constants between FAAs and different oxidants from nitrate photolysis can further help quantify the contribution of nitrate photolysis in FAA degradation and improve the prediction of the atmospheric lifetime of FAAs. The reactivity analysis in concentrated systems is complex, and our experimental results can provide valuable data to parameterize the complex thermodynamics in future studies. Systematic studies of the detailed molecular mechanism and the factors influencing nitrate photochemistry and FAA decay, such as molecular configuration, alkalinity, and solvation are recommended. Quantum chemical and molecular dynamic simulations with appropriate parameters would be useful tools for this purpose.

Data availability. The data used in this study will be made available upon request to the corresponding author.

Supplement. The supplement related to this article is available online at: https://doi.org/10.5194/acp-23-9585-2023-supplement.

Author contributions. ZL and CKC conceptualized the study. ZL, ZC, RZ, and YQ performed the experiments and analyzed the data. ZL wrote the paper. ZL, ZC, RZ, YQ, and CKC reviewed and edited the paper.

Competing interests. The contact author has declared that none of the authors has any competing interests.

Disclaimer. Publisher's note: Copernicus Publications remains neutral with regard to jurisdictional claims in published maps and institutional affiliations.

Financial support. This research has been supported by the Hong Kong Research Grants Council (grant nos. 11314222 and R1016-20F) and the National Natural Science Foundation of China (grant nos. 42275104 and 41905122).

Review statement. This paper was edited by Sergey A. Nizkorodov and reviewed by three anonymous referees.

References

Acero, J. L., Stemmler, K., and Von Gunten, U.: Degradation kinetics of atrazine and its degradation products with ozone and OH radicals: a predictive tool for drinking water treatment, Environ. Sci. Technol., 34, 591–597, 2000.

Aikens, C. M. and Gordon, M. S.: Incremental Solvation of Nonionized and Zwitterionic Glycine, J. Am. Chem. Soc., 128, 12835–12850, https://doi.org/10.1021/ja062842p, 2006.

Asher, S. A., Tuschel, D. D., Vargson, T. A., Wang, L., and Geib, S. J.: Solid state and solution nitrate photochemistry: photochemical evolution of the solid state lattice, J. Phys. Chem. A, 115, 4279–4287, 2011.

Ashraf, H., Guo, Y., Wang, N., Pang, S., and Zhang, Y.-H.: Hygroscopicity of Hofmeister Salts and Glycine Aerosols–Salt Specific Interactions, J. Phys. Chem. A, 125, 1589–1597, https://doi.org/10.1021/acs.jpca.0c10710, 2021.

Aziz, E. F., Ottosson, N., Eisebitt, S., Eberhardt, W., Jagoda-Cwiklik, B., Vácha, R., Jungwirth, P., and Winter, B.: Cation-Specific Interactions with Carboxylate in Amino Acid and Acetate Aqueous Solutions: X-ray Absorption and ab initio Calculations, J. Phys. Chem. B, 112, 12567–12570, https://doi.org/10.1021/jp805177v, 2008.

Benedict, K. B., McFall, A. S., and Anastasio, C.: Quantum yield of nitrite from the photolysis of aqueous nitrate above 300 nm, Environ. Sci. Technol., 51, 4387–4395, 2017.

Berger, P., Karpel Vel Leitner, N., Doré, M., and Legube, B.: Ozone and hydroxyl radicals induced oxidation of glycine, Water Res., 33, 433–441, https://doi.org/10.1016/S0043-1354(98)00230-9, 1999.

Bianco, A., Passananti, M., Perroux, H., Voyard, G., Mouchel-Vallon, C., Chaumerliac, N., Mailhot, G., Deguillaume, L., and Brigante, M.: A better understanding of hydroxyl radical photochemical sources in cloud waters collected at the puy de Dôme station – experimental versus modelled formation rates, Atmos. Chem. Phys., 15, 9191–9202, https://doi.org/10.5194/acp-15-9191-2015, 2015.

Buxton, G. V., Greenstock, C. L., Helman, W. P., and Ross, A. B.: Critical Review of rate constants for reactions of hydrated electrons, hydrogen atoms and hydroxyl radicals (·OH/·O- in Aqueous Solution, J. Phys. Chem. Ref. Data, 17, 513–886, https://doi.org/10.1063/1.555805, 1988.

Case, D. R., Zubieta, J., and P. Doyle, R.: The Coordination Chemistry of Bio-Relevant Ligands and Their Magnesium Complexes, Molecules, 25, 3172, 2020.

Chan, C. K. and Yao, X.: Air pollution in mega cities in China, Atmos. Environ., 42, 1–42, https://doi.org/10.1016/j.atmosenv.2007.09.003, 2008.

Chan, M. N., Choi, M. Y., Ng, N. L., and Chan, C. K.: Hygroscopicity of Water-Soluble Organic Compounds in Atmospheric Aerosols: Amino Acids and Biomass Burning Derived Organic Species, Environ. Sci. Technol., 39, 1555–1562, https://doi.org/10.1021/es049584l, 2005.

Cheng, Z., Luo, L., Wang, S., Wang, Y., Sharma, S., Shimadera, H., Wang, X., Bressi, M., de Miranda, R. M., Jiang, J., Zhou, W., Fajardo, O., Yan, N., and Hao, J.: Status and characteristics of ambient $PM_{2.5}$ pollution in global megacities, Environ. Int., 89–90, 212–221, https://doi.org/10.1016/j.envint.2016.02.003, 2016.

Clegg, S. L., Brimblecombe, P., and Wexler, A. S.: Thermodynamic model of the system H^+- NH_4^+–Na^+–SO_4^{2-}–NO_3^-–Cl^-–H_2O at 298.15 K, J. Phys. Chem. A, 102, 2155–2171, 1998.

Craig, R. L., Peterson, P. K., Nandy, L., Lei, Z., Hossain, M. A., Camarena, S., Dodson, R. A., Cook, R. D., Dutcher, C. S., and Ault, A. P.: Direct determination of aerosol pH: Size-resolved measurements of submicrometer and supermicrometer aqueous particles, Anal. Chem., 90, 11232–11239, 2018.

De Haan, D. O., Hawkins, L. N., Kononenko, J. A., Turley, J. J., Corrigan, A. L., Tolbert, M. A., and Jimenez, J. L.: Formation of Nitrogen-Containing Oligomers by Methylglyoxal and Amines in Simulated Evaporating Cloud Droplets, Environ. Sci. Technol., 45, 984–991, https://doi.org/10.1021/es102933x, 2011.

Furić, K., Mohaček, V., Bonifačić, M., and Štefanić, I.: Raman spectroscopic study of H2O and D2O water solutions of glycine, J. Mol. Struct., 267, 39–44, https://doi.org/10.1016/0022-2860(92)87006-H, 1992.

Gao, S., Xu, B., Zheng, X., Wan, X., Zhang, X., Wu, G., and Cong, Z.: Developing an analytical method for free amino acids in atmospheric precipitation using gas chromatography coupled with mass spectrometry, Atmos. Res., 256, 105579, https://doi.org/10.1016/j.atmosres.2021.105579, 2021.

Gen, M., Zhang, R., Huang, D. D., Li, Y., and Chan, C. K.: Heterogeneous SO_2 Oxidation in Sulfate Formation by Photolysis of Particulate Nitrate, Environ. Sci. Tech. Let., 6, 86–91, https://doi.org/10.1021/acs.estlett.8b00681, 2019.

Gen, M., Liang, Z., Zhang, R., Go Mabato, B. R., and Chan, C. K.: Particulate nitrate photolysis in the atmosphere, Environ. Sci. Atmos., 2, 111–127, https://doi.org/10.1039/D1EA00087J, 2022.

George, C., Ammann, M., D'Anna, B., Donaldson, D. J., and Nizkorodov, S. A.: Heterogeneous photochemistry in the atmosphere, Chem. Rev., 115, 4218–4258, https://doi.org/10.1021/cr500648z, 2015.

Gujarati, V. P., Deshpande, M., Patel, K., and Chaki, S.: Comparitive study of nonlinear semi-organic crystals; glycine sodium nitrate, International Letters of Chemistry, Physics and Astronomy, 61, 12–18, https://doi.org/10.18052/www.scipress.com/ILCPA.61.12, 2015.

Guo, J., Zhou, L., Zen, A., Michaelides, A., Wu, X., Wang, E., Xu, L., and Chen, J.: Hydration of NH_4^+ in Water: Bifurcated Hydrogen Bonding Structures and Fast Rotational Dynamics, Phys. Rev. Lett., 125, 106001, https://doi.org/10.1103/PhysRevLett.125.106001, 2020.

Guo, X., Xiao, H.-S., Wang, F., and Zhang, Y.-H.: Micro-Raman and FTIR spectroscopic observation on the phase transitions of $MnSO_4$ droplets and ionic interactions between Mn^{2+} and SO_4^{2-}, J. Phys. Chem. A, 114, 6480–6486, 2010.

Ha, Z. and Chan, C. K.: The Water Activities of $MgCl_2$, $Mg(NO_3)_2$, $MgSO_4$, and Their Mixtures, Aerosol Sci. Technol., 31, 154–169, https://doi.org/10.1080/027868299304219, 1999.

Haan, D. O. D., Corrigan, A. L., Smith, K. W., Stroik, D. R., Turley, J. J., Lee, F. E., Tolbert, M. A., Jimenez, J. L., Cordova, K. E., and Ferrell, G. R.: Secondary Organic Aerosol-Forming Reactions of Glyoxal with Amino Acids, Environ. Sci. Technol., 43, 2818–2824, https://doi.org/10.1021/es803534f, 2009.

Helin, A., Sietiö, O.-M., Heinonsalo, J., Bäck, J., Riekkola, M.-L., and Parshintsev, J.: Characterization of free amino acids, bacteria and fungi in size-segregated atmospheric aerosols in boreal forest: seasonal patterns, abundances and size distributions, Atmos. Chem. Phys., 17, 13089–13101, https://doi.org/10.5194/acp-17-13089-2017, 2017.

Hu, W., Wang, Z., Huang, S., Ren, L., Yue, S., Li, P., Xie, Q., Zhao, W., Wei, L., and Ren, H.: Biological aerosol particles in polluted regions, Current Pollution Reports, 6, 65–89, 2020.

Ishizuka, S., Reich, O., David, G., and Signorell, R.: Photo-induced shrinking of aqueous glycine aerosol droplets, Atmos. Chem. Phys., 23, 5393–5402, https://doi.org/10.5194/acp-23-5393-2023, 2023.

Jentzsch, P. V., Kampe, B., Ciobotă, V., Rösch, P., and Popp, J.: Inorganic salts in atmospheric particulate matter: Raman spectroscopy as an analytical tool, Spectrochim. Acta A, 115, 697–708, 2013.

Kitada, K., Suda, Y., and Takenaka, N.: Cyanide Formation in Freezer Stored Foods: Freezing of a Glycine and Nitrite Mixture, Chem. Res. Toxicol., 33, 1809–1814, https://doi.org/10.1021/acs.chemrestox.0c00054, 2020.

Krauklis, I. V., Tulub, A. V., Golovin, A. V., and Chelibanov, V. P.: Raman Spectra of Glycine and Their Modeling in Terms of the Discrete–Continuum Model of Their Water Solvation Shell, Optics and Spectroscopy, 128, 1598–1601, https://doi.org/10.1134/S0030400X20100161, 2020.

Kristensson, A., Rosenørn, T., and Bilde, M.: Cloud droplet activation of amino acid aerosol particles, J. Phys. Chem. A, 114, 379–386, 2010.

Kumar, S., Rai, A. K., Singh, V. B., and Rai, S. B.: Vibrational spectrum of glycine molecule, Spectrochim. Acta A, 61, 2741–2746, https://doi.org/10.1016/j.saa.2004.09.029, 2005.

Lester, G. E., Jifon, J. L., and Makus, D. J.: Impact of potassium nutrition on postharvest fruit quality: Melon (*Cucumis melo* L) case study, Plant Soil, 335, 117–131, 2010.

Li, X., Zhang, Y., Shi, L., Kawamura, K., Kunwar, B., Takami, A., Arakaki, T., and Lai, S.: Aerosol Proteinaceous Matter in Coastal Okinawa, Japan: Influence of Long-Range Transport and Photochemical Degradation, Environ. Sci. Technol., 56, 5256–5265, https://doi.org/10.1021/acs.est.1c08658, 2022.

Li, Y., Geng, Y., Hu, X., and Yin, X.: Seasonal differences in sources and formation processes of $PM_{2.5}$ nitrate in an urban environment of North China, J. Environ. Sci., 120, 94–104, https://doi.org/10.1016/j.jes.2021.08.020, 2022.

Liang, Z., Zhang, R., Gen, M., Chu, Y., and Chan, C. K.: Nitrate Photolysis in Mixed Sucrose–Nitrate–Sulfate Particles at Different Relative Humidities, J. Phys. Chem. A, 125, 3739–3747, https://doi.org/10.1021/acs.jpca.1c00669, 2021.

Liang, Z., Chu, Y., Gen, M., and Chan, C. K.: Single-particle Raman spectroscopy for studying physical and chemical processes of atmospheric particles, Atmos. Chem. Phys., 22, 3017–3044, https://doi.org/10.5194/acp-22-3017-2022, 2022a.

Liang, Z., Chan, W. L., Tian, X., Lai, A. C. K., Lee, P. K. H., and Chan, C. K.: Inactivation of Escherichia coli in droplets at different ambient relative humidities: Effects of phase transition, solute and cell concentrations, Atmos. Environ., 280, 119066, https://doi.org/10.1016/j.atmosenv.2022.119066, 2022b.

Liang, Z., Zhou, L., Infante Cuevas, R. A., Li, X., Cheng, C., Li, M., Tang, R., Zhang, R., Lee, P. K. H., Lai, A. C. K., and Chan, C. K.: Sulfate Formation in Incense Burning Particles: A Single-Particle Mass Spectrometric Study, Environ. Sci. Tech. Let., 9, 718–725, https://doi.org/10.1021/acs.estlett.2c00492, 2022c.

Lightstone, J. M., Onasch, T. B., Imre, D., and Oatis, S.: Deliquescence, efflorescence, and water activity in ammonium nitrate and mixed ammonium nitrate/succinic acid microparticles, J. Phys. Chem. A, 104, 9337–9346, 2000.

Ling, T. Y. and Chan, C. K.: Formation and Transformation of Metastable Double Salts from the Crystallization of Mixed Ammonium Nitrate and Ammonium Sulfate Particles, Environ. Sci. Technol., 41, 8077–8083, https://doi.org/10.1021/es071419t, 2007.

Liu, F., Lai, S., Tong, H., Lakey, P. S., Shiraiwa, M., Weller, M. G., Pöschl, U., and Kampf, C. J.: Release of free amino acids upon oxidation of peptides and proteins by hydroxyl radicals, Anal. Bioanal. Chem., 409, 2411–2420, 2017.

Liu, M., Song, Y., Zhou, T., Xu, Z., Yan, C., Zheng, M., Wu, Z., Hu, M., Wu, Y., and Zhu, T.: Fine particle pH during severe haze episodes in northern China, Geophys. Res. Lett., 44, 5213–5221, 2017.

Locke, M. J. and McIver Jr., R. T.: Effect of solvation on the acid/base properties of glycine, J. Am. Chem. Soc., 105, 4226–4232, 1983.

Marsh, A., Miles, R. E. H., Rovelli, G., Cowling, A. G., Nandy, L., Dutcher, C. S., and Reid, J. P.: Influence of organic compound functionality on aerosol hygroscopicity: dicarboxylic acids, alkyl-substituents, sugars and amino acids, Atmos. Chem. Phys., 17, 5583–5599, https://doi.org/10.5194/acp-17-5583-2017, 2017.

Matos, J. T., Duarte, R. M., and Duarte, A. C.: Challenges in the identification and characterization of free amino acids and proteinaceous compounds in atmospheric aerosols: A critical review, TrAC-Trend. Anal. Chem., 75, 97–107, 2016.

Matsumoto, K., Kim, S., and Hirai, A.: Origins of free and combined amino acids in the aerosols at an inland urban site in Japan, Atmos. Environ., 259, 118543, https://doi.org/10.1016/j.atmosenv.2021.118543, 2021.

Matsumura, T. and Hayashi, M.: Hygroscopic Growth of an $(NH_4)_2SO_4$ Aqueous Solution Droplet Measured Using an Environmental Scanning Electron Microscope (ESEM), Aerosol Sci. Technol., 41, 770–774, https://doi.org/10.1080/02786820701436831, 2007.

Medoš, Ž., Plechkova, N. V., Friesen, S., Buchner, R., and Bešter-Rogač, M.: Insight into the Hydration of Cationic Surfactants: A Thermodynamic and Dielectric Study of Functionalized Quaternary Ammonium Chlorides, Langmuir, 35, 3759–3772, https://doi.org/10.1021/acs.langmuir.8b03993, 2019.

Moision, R. M. and Armentrout, P. B.: Experimental and Theoretical Dissection of Sodium Cation/Glycine Interactions, J. Phys. Chem. A, 106, 10350–10362, https://doi.org/10.1021/jp0216373, 2002.

Mopper, K. and Zika, R. G.: Free amino acids in marine rains: evidence for oxidation and potential role in nitrogen cycling, Nature, 325, 246–249, 1987.

Pei, W.-X., Ma, S.-S., Chen, Z., Zhu, Y., Pang, S.-F., and Zhang, Y.-H.: Heterogeneous uptake of NO_2 by sodium acetate droplets and secondary nitrite aerosol formation, J. Environ. Sci., 127, 320–327, https://doi.org/10.1016/j.jes.2022.05.048, 2023.

Philipsen, P., Knudsen, L., Gniadecka, M., Ravnbak, M., and Wulf, H.: Diagnosis of malignant melanoma and basal cell carcinoma by in vivo NIR-FT Raman spectroscopy is independent of skin pigmentation, Photoch. Photobio. Sci., 12, 770–776, 2013.

Ren, L., Bai, H., Yu, X., Wu, F., Yue, S., Ren, H., Li, L., Lai, S., Sun, Y., Wang, Z., and Fu, P.: Molecular composition and seasonal variation of amino acids in urban aerosols from Beijing, China, Atmos. Res., 203, 28–35, https://doi.org/10.1016/j.atmosres.2017.11.032, 2018.

Scharko, N. K., Berke, A. E., and Raff, J. D.: Release of nitrous acid and nitrogen dioxide from nitrate photolysis in acidic aqueous solutions, Environ. Sci. Technol., 48, 11991–12001, 2014.

Selvarani, K., Mahalakshmi, R., and Srinivasan, N.: Growth and characterization of nonlinear optical crystal glycine sodium nitrate and its biological activity, J. Mater. Sci.-Mater. El., 33, 13408–13417, 2022.

Socrates, G.: Infrared and Raman characteristic group frequencies: tables and charts, John Wiley & Sons, ISBN 978-0-470-09307-8, 2004.

Song, T., Wang, S., Zhang, Y., Song, J., Liu, F., Fu, P., Shiraiwa, M., Xie, Z., Yue, D., Zhong, L., Zheng, J., and Lai, S.: Proteins and Amino Acids in Fine Particulate Matter in Rural Guangzhou, Southern China: Seasonal Cycles, Sources, and Atmospheric Processes, Environ. Sci. Technol., 51, 6773–6781, https://doi.org/10.1021/acs.est.7b00987, 2017.

Stroud, E. D., Fife, D. J., and Smith, G. G.: A method for the determination of the pKa of the. alpha.-hydrogen in amino acids using racemization and exchange studies, J. Org. Chem., 48, 5368–5369, 1983.

Suresh, S., Ramanand, A., Mani, P., and Murthyanand, K.: Growth, structural, optical, mechanical and dielectric properties of glycine sodium nitrate (GSN) single crystal, Journal of Optoelectronics and Biomedical Materials, 1, 129–139, 2010.

Surovtsev, N., Adichtchev, S., Malinovsky, V., Ogienko, A., Drebushchak, V., Manakov, A. Y., Ancharov, A., Yunoshev, A., and Boldyreva, E.: Glycine phases formed from frozen aqueous solutions: Revisited, J. Chem. Phys., 137, 065103, https://doi.org/10.1063/1.4739532, 2012.

Tang, I. N.: Thermodynamic and optical properties of mixed-salt aerosols of atmospheric importance, J. Geophys. Res.-Atmos., 102, 1883–1893, https://doi.org/10.1029/96JD03085, 1997.

Tang, N. and Skibsted, L. H.: Calcium Binding to Amino Acids and Small Glycine Peptides in Aqueous Solution: Toward Peptide Design for Better Calcium Bioavailability, J. Agr. Food Chem., 64, 4376–4389, https://doi.org/10.1021/acs.jafc.6b01534, 2016.

Tortonda, F. R., Pascual-Ahuir, J. L., Silla, E., and Tuñón, I.: Why is glycine a zwitterion in aqueous solution? A theoretical study of solvent stabilising factors, Chem. Phys. Lett., 260, 21–26, https://doi.org/10.1016/0009-2614(96)00839-1, 1996.

Venkatesu, P., Lee, M.-J., and Lin, H.-M.: Densities of aqueous solutions containing model compounds of amino acids and ionic salts at $T = 298.15$ K, J. Chem. Thermodyn., 39, 1206–1216, https://doi.org/10.1016/j.jct.2006.11.014, 2007.

Vimalan, M., Flora, X. H., Tamilselvan, S., Jeyasekaran, R., Sagayaraj, P., and Mahadevan, C.: Optical, thermal, mechanical and electrical properties of a new NLO material: Mono-L-alaninium nitrate (MAN), Arch. Phys. Res., 1, 44–53, 2010.

Wang, N., Guo, Y., Li, J., Pang, S., and Zhang, Y.: Hygroscopic behavior and phase state of mixed NH4NO3 /amino acids particles by microscopy and IR technology, Atmos. Environ., 273, 118951, https://doi.org/10.1016/j.atmosenv.2022.118951, 2022.

Wang, P., Wang, N., Pang, S.-F., and Zhang, Y.-H.: Hygroscopicity of internally mixed particles glycine/$NaNO_3$ studied by FTIR-ATR technique, J. Aerosol Sci., 116, 25–33, https://doi.org/10.1016/j.jaerosci.2017.11.013, 2018.

Weber, R. J., Guo, H., Russell, A. G., and Nenes, A.: High aerosol acidity despite declining atmospheric sulfate concentrations over the past 15 years, Nat. Geosci., 9, 282–285, 2016.

Wen, L., Schaefer, T., Zhang, Y., He, L., Ventura, O. N., and Herrmann, H.: T- and pH-dependent OH radical reaction kinetics with glycine, alanine, serine, and threonine in the aqueous phase, Phys. Chem. Chem. Phys., 24, 11054–11065, https://doi.org/10.1039/D1CP05186E, 2022.

Xu, Y., Wu, D., Xiao, H., and Zhou, J.: Dissolved hydrolyzed amino acids in precipitation in suburban Guiyang, southwestern China: Seasonal variations and potential atmospheric processes, Atmos. Environ., 211, 247–255, 2019.

Xuan, X., Chen, Z., Gong, Y., Shen, H., and Chen, S.: Partitioning of hydrogen peroxide in gas-liquid and gas-aerosol phases, Atmos. Chem. Phys., 20, 5513–5526, https://doi.org/10.5194/acp-20-5513-2020, 2020.

Zhang, Q. and Anastasio, C.: Free and combined amino compounds in atmospheric fine particles ($PM_{2.5}$) and fog waters from Northern California, Atmos. Environ., 37, 2247–2258, https://doi.org/10.1016/S1352-2310(03)00127-4, 2003.

Zhang, R., Gen, M., Fu, T.-M., and Chan, C. K.: Production of Formate via Oxidation of Glyoxal Promoted by Particulate Nitrate Photolysis, Environ. Sci. Technol., 55, 5711–5720, https://doi.org/10.1021/acs.est.0c08199, 2021.

Zhang, R., Gen, M., Liang, Z., Li, Y. J., and Chan, C. K.: Photochemical Reactions of Glyoxal during Particulate Ammonium Nitrate Photolysis: Brown Carbon Formation, Enhanced Glyoxal Decay, and Organic Phase Formation, Environ. Sci. Technol., 56, 1605–1614, https://doi.org/10.1021/acs.est.1c07211, 2022.

Zhu, R.-G., Xiao, H.-Y., Zhu, Y., Wen, Z., Fang, X., and Pan, Y.: Sources and Transformation Processes of Proteinaceous Matter and Free Amino Acids in $PM_{2.5}$, J. Geophys. Res.-Atmos., 125, e2020JD032375, https://doi.org/10.1029/2020JD032375, 2020.

Zhu, R.-G., Xiao, H.-Y., Luo, L., Xiao, H., Wen, Z., Zhu, Y., Fang, X., Pan, Y., and Chen, Z.: Measurement report: Hydrolyzed amino acids in fine and coarse atmospheric aerosol in Nanchang, China: concentrations, compositions, sources and possible bacterial degradation state, Atmos. Chem. Phys., 21, 2585–2600, https://doi.org/10.5194/acp-21-2585-2021, 2021.

Zhuang, H., Chan, C. K., Fang, M., and Wexler, A. S.: Size distributions of particulate sulfate, nitrate, and ammonium at a coastal site in Hong Kong, Atmos. Environ., 33, 843–853, https://doi.org/10.1016/S1352-2310(98)00305-7, 1999a.

Zhuang, H., Chan, C. K., Fang, M., and Wexler, A. S.: Formation of nitrate and non-sea-salt sulfate on coarse particles, Atmos. Environ., 33, 4223–4233, https://doi.org/10.1016/S1352-2310(99)00186-7, 1999b.

Zuend, A., Marcolli, C., Booth, A. M., Lienhard, D. M., Soonsin, V., Krieger, U. K., Topping, D. O., McFiggans, G., Peter, T., and Seinfeld, J. H.: New and extended parameterization of the thermodynamic model AIOMFAC: calculation of activity coefficients for organic-inorganic mixtures containing carboxyl, hydroxyl, carbonyl, ether, ester, alkenyl, alkyl, and aro-

matic functional groups, Atmos. Chem. Phys., 11, 9155–9206, https://doi.org/10.5194/acp-11-9155-2011, 2011.